Magnetometer based on a quartz MEMS resonator with two DETFs and a stack of magnetic materials

Charles Mauc
ONERA
C2N
Chatillon, France
charles.mauc@onera.fr

Thomas Perrier
ONERA
Chatillon, France
thomas.perrier@onera.fr

Raphaël Levy
ONERA
Chatillon, France
raphael.levy@onera.fr

Johan Moulin
C2N
Palaiseau, France
johan.moulin@u-psud.fr

Patrick Kayser
ONERA
Chatillon, France
patrick.kayser@onera.fr

Abstract — This paper presents a resonating quartz MEMS magnetometer exploiting the torque induced by the external magnetic field on a stack of ferromagnetic and antiferromagnetic materials and the differential measurement of the resonance frequencies of two DETFs. It is targeted for applications such as magneto-inertial navigation. This sensor was fabricated using a wet HF/NH_4F etching process and its working principle was proven correct with a magnetic sensitivity of 770 Hz/T.

Keywords — Magnetometer, IMU, MEMS, quartz, DETF, exchange bias

I. INTRODUCTION

Inertial navigation addresses the problem of estimating the motion of a rigid body with respect to an inertial frame of reference. For this application, there are several ways to use a magnetometer. First, they can be used to correct the bias of gyroscopes by finding the magnetic north [1]. They can also be integrated into Inertial Measurement Unit (IMU) as a support function of the gyroscopes and accelerometers to do magneto-inertial navigation [2]. By making the assumptions that the surrounding magnetic field $\boldsymbol{B}$ is non-uniform and does not depend on time, with a magnetometer able to measure the magnetic field $\boldsymbol{B}$ and its gradient $\nabla\boldsymbol{B}$, one will be able to deduce its velocity and position [2].

For embedded applications, there are different technologies of magnetic sensors available like Hall sensors, AMR, fluxgates and MEMS magnetometers. Among the latter, the majority uses the Lorentz force $\boldsymbol{F} = q \cdot (\boldsymbol{E} + \boldsymbol{v} \times \boldsymbol{B})$ as their core mechanism [3] [4], while other exploit the magnetostriction [5] or the torque incited by a magnetic field on a magnetic moment [6].

This paper will introduce a new design of vectorial magnetometer taking advantage of a MEMS resonator with a frequency output and a stack of ferromagnetic (FM) and antiferromagnetic (AFM) materials. The working principle will be introduced, then the design of the resonator will be discussed and finally the experimental results of the sensitivity to the magnetic field will be presented.

II. WORKING PRINCIPLE

The device (Fig. 1) is made out of one piece of quartz. There are three parts assuming different functions. First, there are two beams (in grey) used as a differential force sensor. They are vibrating in flexural mode at their resonance frequencies f_{R1} and f_{R2}, and actuated by three electrodes each. They are directly linked to the second part being a large surface (in red) where magnetic materials are deposited. It is assumed that the magnetic materials have a homogeneous and unidirectional magnetization $\boldsymbol{M} = M \cdot \boldsymbol{e_x}$. Finally, there is the pivot (in white) that allows the surface to rotate around it.

When the surrounding magnetic field $\boldsymbol{B} = B_x \cdot \boldsymbol{e_x} + B_y \cdot \boldsymbol{e_y} + B_z \cdot \boldsymbol{e_z}$ interacts with the magnetic moment $\boldsymbol{m} = m \cdot \boldsymbol{e_x}$ of magnetic materials, the torque $\boldsymbol{\Gamma}$ appears and makes the surface rotate around $\boldsymbol{e_x}$ and $\boldsymbol{e_z}$ such as:

$$\boldsymbol{\Gamma} = \boldsymbol{m} \times \boldsymbol{B} = V_{magn} \cdot \boldsymbol{M} \times \boldsymbol{B} = \Gamma_y \cdot \boldsymbol{e_y} + \Gamma_z \cdot \boldsymbol{e_z} \quad (1)$$

Where $\boldsymbol{m}$ is the magnetic moment of the magnetic materials and V_{magn} is the volume of the FM material.

As a consequence, when the surface experiences Γ_y, the surface rotates around the pivot and will compress one beam and stretch the other one with the same force $\boldsymbol{F} = \pm F \cdot \boldsymbol{e_z}$ because the beams are symmetrically distributed (Fig. 1). It is leading to an opposite variation of the resonance frequencies of the two beams [7]. It is then possible to find a proportional relation between B_y and the difference of resonance frequencies of the two beams:

$$\Delta f = f_{R1} - f_{R2} = K_B \cdot B_y \quad (2)$$

$$K_B \propto M \cdot V_{magn} \cdot 1/(b_p^2 \cdot h_p \cdot d) \quad (3)$$

Where K_B is the scale factor or magnetic sensitivity, d the distance between the two beams, b_p the width of a beam and h_p the thickness of the structure.

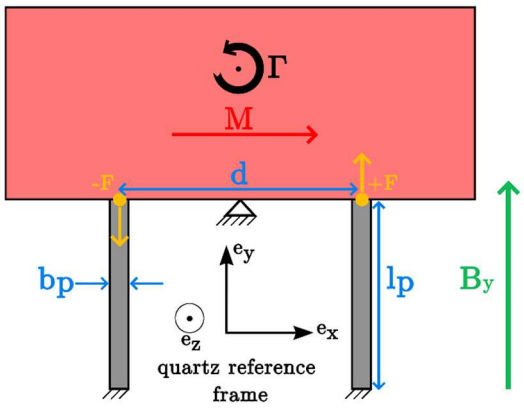

Fig. 1. Working principle of the resonator

The advantage one gets when one takes advantage of a differential measurement such as Δf is to reduce a lot the influence of environmental factors like temperature, acceleration, rotation and vibrations, which make the resonance frequencies of the beams change likewise. It is then possible to estimate the resolution of such a device thanks to [8]:

$$\sigma(\tau) \propto f_R/Q \cdot K_B \quad (4)$$

On the other hand, the torque component Γ_z will deflect the surface around $\boldsymbol{e_x}$. However, the pivot maintains the beams in the (XY) plan which will prevent them from bending too much, and the residual resonance frequency shift is the same for both beams and so will be also reduced a lot by the differential Δf.

III. Design of the Magnetometer

To get to the design of the MEMS resonator which will provide at the same time a very low resolution (< 10 nT) and will be a less sensitive as possible of the environmental factors, simulations were undertaken with a CAE software and the Oofelie::Multiphysics solver.

A. Choice of the structure material

For this MEMS magnetometer, we chose to use α-quartz instead of silicon because the temperature sensitivity of a Si resonator is much higher than a quartz resonator. Then, among all the quartz's cuts, we opted for the z-cut of the quartz because it allows a fast and relatively clean wet chemical etching, and because it is fitted for low frequency versus temperature sensitivity of the flexural mode at low frequency when the beams are in the Y direction [9].

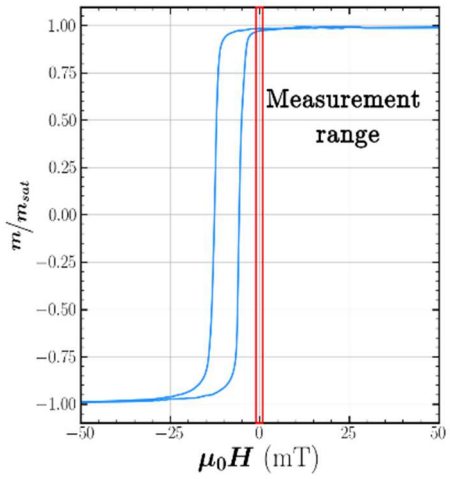

Fig. 2. Hysteresis loop of a ten bilayers NiMn/$Co_{35}Fe_{65}$ stack

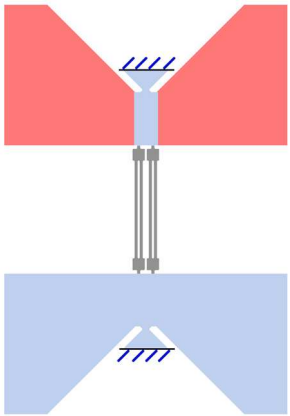

Fig. 3. Symmetrical design along the X-axis and Y-axis

B. Magnetic materials

To have a constant magnetization all over the measurement scale $[-0.1\text{ mT}; 0.1\text{ mT}]$, it is not possible to use a single ferromagnetic material because the minor hysteresis loops can lead to a variation of the magnetization and even a demagnetization of the material [10]. Therefore, we decided to take advantage of the interaction between the atomic magnetic moments of a ferromagnetic material and an antiferromagnetic material after a field cooling procedure [11]. This exchange interaction can shift the hysteresis loop in the direction of the magnetic field applied during the field cooling procedure to the point where $\boldsymbol{M} = M_{sat} \cdot \boldsymbol{e_x}$ on the measurement scale (Fig. 2).

The combination of NiMn as for the AFM material and $Co_{35}Fe_{65}$ as for the FM material in the stack {NiCr (20nm) + [NiMn (50 nm) / $Co_{35}Fe_{65}$ (50 nm)]$_{10}$ + NiMn (50 nm)} allows to maximise the number of interfaces and have the greatest exchange energy after a non-standard field cooling procedure [12].

C. Design of the vibrating beams

To avoid the "lock-in" phenomenon, which is referring to the mechanical coupling between two beams when they tend to vibrate at the same resonance frequency [13], double-ended tuning forks (DETFs) were designed. Among one DETF, the two beams have a great mechanical coupling due to their proximity, forcing them to vibrate at the same resonance frequency. If they vibrate in their anti-phase vibratory mode, the elastic strain waves produced by each beam within the DETF will cancel out in the DETF's anchor [14], which will lead to the mechanical isolation of the two DETFs of this differential magnetometer.

D. Design of the structure

If the design was fabricated with no defect, the differential measurement should cancel the influences of the parasitic sensitivities thanks to the proximity of the DETFs and the perfect symmetry of the structure. In practice, there are slight dissymmetries in the structure and between the beams due to the fabrication process. In consequence, the magnetometer is sensitive to rotation and particularly to acceleration.

To be as less sensitive as possible to the latter, the vibrating beams should be as less stress as possible when the structure wraps in order not to change their resonance frequencies. Therefore, the design of such a structure should be symmetrical along the X-axis and Y-axis and the two anchor points of a DETF should be similar (Fig. 3).

The magnetic sensitivity K_B of this design is lessen in comparison with a design where one of the anchor points of each DETF is fixed. Indeed, when a magnetic field makes the upper plate rotates, the lower plate also rotates which leads to a lesser extension/compression of the DETFs.

E. Design of the pivot

This pivot is a crucial part of the magnetometer because it allows the plates to rotate around it and maintains the structure when subjected to an acceleration or a rotation. A pivot can be physical or can result from a geometrical construction (Fig. 4). The latter offers a rotation without

mechanical loss, however it implies that the anchor points of the DETFs are different given the needs for the magnetometer, so, we opted for a physical pivot. We chose to test three different designs of pivot: one is "full", one has two branches and one has three branches, with different branch lengths and different widths between the branches (Fig. 5). Out of the three pivots, the 500 µm "full" pivot grants the best compromise between a high K_B and a low sensitivity to acceleration (Fig. 6, Fig. 7).

F. *Fabrication process*

To fabricate the resonator, we used a wet HF/NH_4F etching process on a 210 µm thick quartz wafer. This process leads to the apparition of etching facets on the sidewalls because the quartz has different etch-rates depending of its crystallographic orientation [9]. Due to the increase of the cross-section of the beams and due to the bad etching of the areas where there are many corners such as the heads of the DETFs, the magnetic sensitivity is lessen. Furthermore, the sidewalls are not perfectly homogeneous so the resonance frequency and the quality factor of a DETF vary between the two DETFs of a resonator.

The magnetic materials are sputtered through a physical mask aligned thanks to two visual alignment markers. Then the MEMS structure with the magnetic materials is annealed to obtain an homogenous magnetization $M = M_{sat}$.

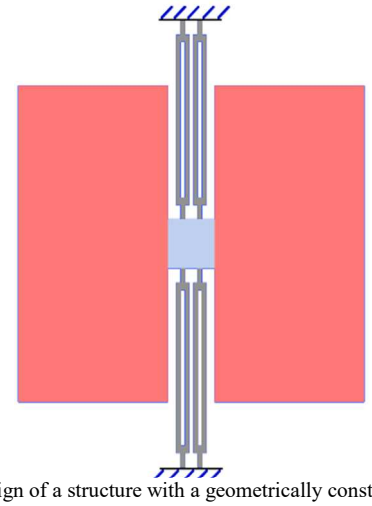

Fig. 4. Design of a structure with a geometrically constructed pivot

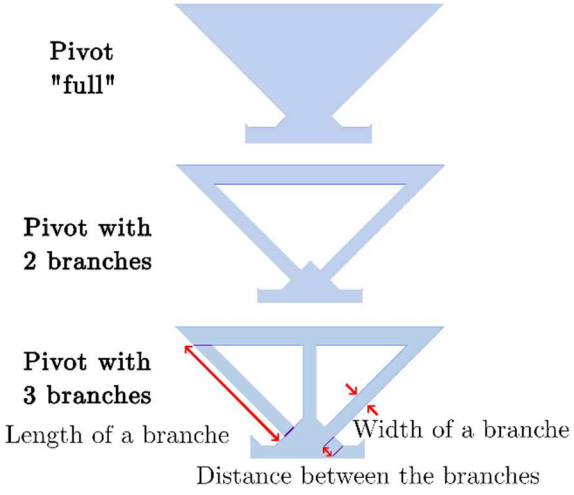

Fig. 5. Three designs of pivot

G. *Integration and proximity circuits*

The magnetometer is fixed on a ceramic base and sealed with a copper bonnet in order to work under vacuum (Fig. 8). The package goes through several thermal cycles to release the gas that may be trapped and relax the magnetic materials' internal stress.

To track the resonance frequency of one DETF over time, it is not conceivable to do a frequency sweep to find the resonance, so we use a servo-loop on the phase or Phase Locked Loop (PLL) of the electric signal coming from the electrodes, this is the role of the oscillator circuit fulfilled by an HF2LI. An input electric signal is applied on the *drive* electrode, an output signal is retrieved on the *sense* electrode, and the third electrode is connected to the electrical mass to avoid capacitive coupling. We also need to use a charge amplifier circuit to amplify the electric signal coming from the *sense* electrode because of the low piezoelectric coupling factor of the quartz [15] (Fig. 8).

IV. Experimental Results

To prove the working principle to be correct, we impose a square wave magnetic field with 5 seconds periods. It is generated thanks to a Helmholtz coil and set to be perpendicular to the magnetization and within the plan of the magnetometer. We can observe the resonance frequencies of

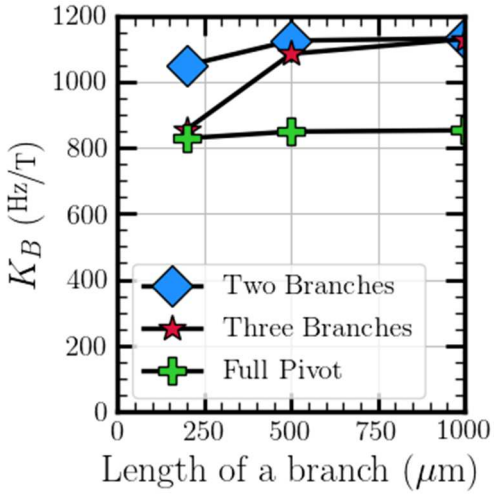

Fig. 6. Magnetic sensitivity $\boldsymbol{K_B}$ in function of the length of a branch of the pivot

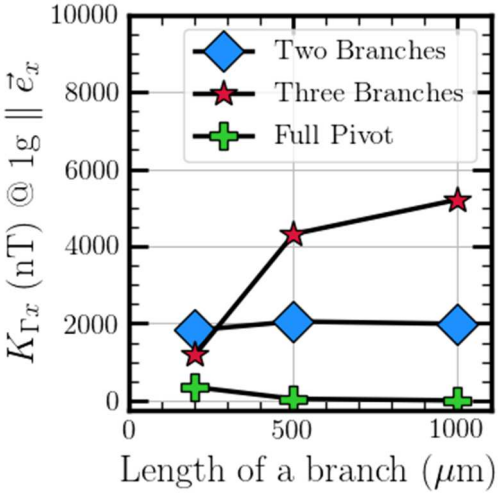

Fig. 7. Sensitivity to an acceleration of 1g along the X axis $\boldsymbol{K_\Gamma}$ in function of the length of a branch of the pivot

the two DETFs: f_{R1} and f_{R2} each varying oppositely of approximatively ± 0.25 Hz for a ≈ 0.6 mT variation measured with a Hall probe. It confirms that the magnetometer is working in accordance with its working principle. It is then possible to estimate the magnetic sensitivity to $K_B = 770$ Hz/T (Fig. 9). Furthermore, we can notice the resonance frequencies f_{R1} and f_{R2} not to be steady even when the magnetic field is turned off. It is due to environmental factors and, in this case, the variation of temperature in the room where the measurement was done. We can also notice that the variations of resonance frequencies are the same for f_{R1} and f_{R2}. This is why the calculated magnetic field $B = \Delta f / K_B$ is so flat: the differential reduced a lot the influence of the temperature which acts as a common mode bias.

CONCLUSION

A new type of MEMS magnetic sensor with frequency output was designed thanks to an analytical model and a finite element software. The experimental measurements validate the working principle with a measured magnetic sensitivity of $K_B = 770$ Hz/T in accordance with theoretical model.

The remaining characterisations, which are the sensitivities over temperature, acceleration, rotation speed and to the other components of the magnetic field, will soon be measured and an FPGA is shortly expected in order to have a fully embedded magnetometer.

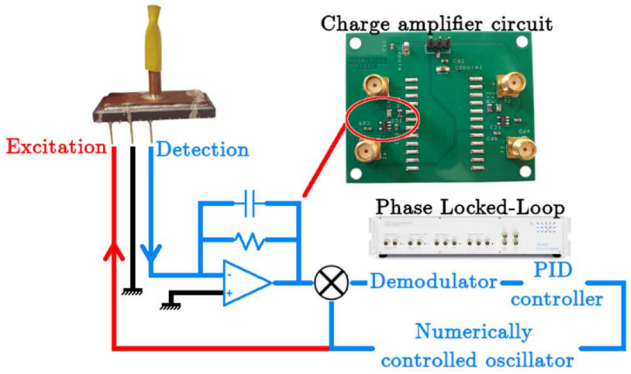

Fig. 8. Packaged magnetometer with its charge amplifier circuit and its PLL circuit

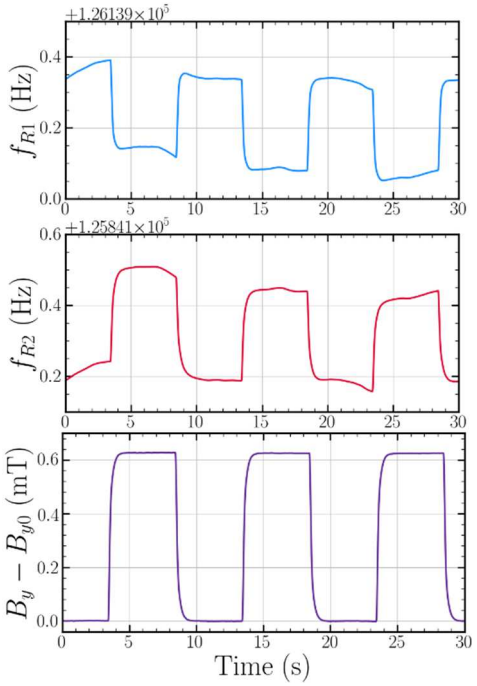

Fig. 9. Resonance frequencies f_{R1} (Hz) and f_{R2} (Hz) of the two DETFs and the calculated variation of magnetic field in comparison with the surrounding magnetic field (mT) in function of time

ACKNOWLEDGMENT

This study is part of a PhD thesis under funding from AID/DGA (Defense Innovation Agency - French MoD) and was supported by the French ANR program Astrid Maturation (ANR-19-ASMA-0002-01). The authors would like to thank AID/DGA for their support.

REFERENCES

[1] A. Yurtman and B. Barshan, "Novel Noniterative Orientation Estimation for Wearable Motion Sensor Units Acquiring Accelerometer, Gyroscope, and Magnetometer Measurements," *IEEE Trans. Instrum. Meas.*, vol. 69, no. 6, pp. 3206–3215, 2020.

[2] E. Dorveaux, "Navigation Magnéto-Inertielle Principes et application à un système podométrique indoor," Mines ParisTech, 2012.

[3] J. Kyynäräinen *et al.*, "A 3D micromechanical compass," *Sensors Actuators, A Phys.*, vol. 142, no. 2, pp. 561–568, 2008.

[4] A. Herrera-May, J. Soler-Balcazar, H. Vázquez-Leal, J. Martínez-Castillo, M. Vigueras-Zuñiga, and L. Aguilera-Cortés, "Recent Advances of MEMS Resonators for Lorentz Force Based Magnetic Field Sensors: Design, Applications and Challenges," *Sensors*, vol. 16, no. 9, p. 1359, Aug. 2016.

[5] L. Bian *et al.*, "A Resonant Magnetic Field Sensor with High Quality Factor Based on Quartz Crystal Resonator and Magnetostrictive Stress Coupling," *IEEE Trans. Electron Devices*, vol. 65, no. 6, pp. 2585–2591, 2018.

[6] D. Ettelt, P. Rey, G. Jourdan, A. Walther, P. Robert, and J. Delamare, "3D magnetic field sensor concept for use in inertial measurement units (IMUs)," *J. Microelectromechanical Syst.*, vol. 23, no. 2, pp. 324–333, 2014.

[7] "IEEE Standard Specification Format Guide and Test Procedure for Linear Single-Axis, Nongyroscopic Accelerometers," *IEEE Stand. 1293-2018*, pp. 1–271, 2019.

[8] R. Levy and V. Gaudineau, "Phase noise analysis and performance of the Vibrating Beam Accelerometer," *2010 IEEE Int. Freq. Control Symp. FCS 2010*, pp. 511–514, 2010.

[9] P. Rangsten, C. Hedlund, I. V. Katardjiev, and Y. Bäcklund, "Etch rates of crystallographic planes in Z-cut quartz - Experiments and simulation," *J. Micromechanics Microengineering*, vol. 8, no. 1, pp. 1–6, 1998.

[10] E. Du Trémolet de Lacheisserie, *Magnetism I - Fondements*, Grenoble S. 1999.

[11] J. Nogués *et al.*, "Exchange bias in nanostructures," *Phys. Rep.*, vol. 422, no. 3, pp. 65–117, 2005.

[12] C. Mauc, T. Perrier, J. Moulin, and P. Kayser, "Induced exchange bias in NiMn/CoFe multilayer thin films sputtered on a quartz substrate by field cooling," *J. Magn. Magn. Mater.*, vol. 544, no. September 2021, p. 168649, Feb. 2022.

[13] O. Le Traon, D. Janiaud, B. Lecorre, M. Pernice, S. Muller, and J. Y. Tridera, "Monolithic differential vibrating beam accelerometer within an isolating system between the two resonators," *Proc. IEEE Sensors*, vol. 2005, pp. 648–651, 2005.

[14] M. Zhang, G. Luiz, S. Shah, G. Wiederhecker, and M. Lipson, "Eliminating anchor loss in optomechanical resonators using elastic wave interference," *Appl. Phys. Lett.*, vol. 105, no. 5, 2014.

[15] R. Abdolvand, H. Fatemi, and S. Moradian, "Quality Factor and Coupling in Piezoelectric MEMS Resonators," H. Bhugra and G. Piazza, Eds. Cham: Springer International Publishing, 2017, pp. 133–152.